RSC Advances

ROYAL SOCIETY OF CHEMISTRY

www.rsc.org/advances

Starch nanoparticles prepared in two ionic liquids based microemulsion system and their drug loading and release properties

Xinge Wang[1], Jianhua Cheng[2], Guangyin Ji[1], Xichun Peng[3], Zhigang Luo[1]*

1.Carbohydrate Lab, College of Food Science, South China University of Technology, Guangzhou, 510640, China; 2.Ministry of Education Key Laboratory of Pollution Control and Ecological Remediation for Industrial Agglomeration Area, College of Environment and Energy, South China University of Technology, Guangzhou 510006, China;3. Department of Food Science and Engineering, College of Science and Engineering, Jinan University, Guangzhou 510632, China

*Corresponding author:

Zhigang Luo, Tel: +86-20-87113845, Fax: +86-20-87113848. E-mail address: zhgluo@scut.edu.cn;

ABSTRACT

In this work, 1-hexadecyl-3-methylimidazolium bromide ([C_{16}mim]Br) and 1-octyl-3-methylimidazolium acetate ([C_8mim]Ac) were simultaneously used as substitutes for surfactants and polar phase to prepare [C_{16}mim]Br/butan-1-ol/cyclohexane/[C_8mim]Ac ionic liquid microemulsions. Then, the structure of microemulsion was investigated by pseudo-ternary phase diagram, dynamic light scanning (DLS) and conductivity measurement. Starch nanoparticles with a mean diameter of 80.5 nm were prepared with Octenyl Succinic Anhydride (OSA) starch as raw material through ionic liquid-in-oil (IL/O) microemulsion cross-linking reaction. Scanning electron microscope (SEM) data revealed that starch nanoparticles were spherical granules with small size. In addition, the particles presented homogeneous distribution and no aggregation phenomenon appeared. The results of Fourier transform infrared spectroscopy (FTIR) identified the formation of cross-linking bonds in starch molecules. Finally, the drug loading and releasing properties of starch nanoparticles were investigated with mitoxantrone hydrochloride as drug model. This work might provide an efficient method to synthesis starch nanoparticles.

Keywords: [C_{16}mim]Br; [C_8mim]Ac; Ionic liquid microemulsion; Starch nanoparticles; Drug loading; Drug releasing.

1. Introduction

Starch，a renewable, biodegradable natural polymer with low-cost, has been widely applied to food and industrial fields as thickener, gelling agent, bulking agent and water retention agent.[1-3] However, native starch has limitations such as poor processability and solubility, which limit its industrial application. Therefore, starch can be modified using physical, chemical or enzymatic treatments to improve its properties,[4-6] among which cross-linked starch microspheres show good performance towards swelling, high temperature, high shear and acidic conditions and have been one of the most investigated drug carriers due to their total biodegradability, biocompatibility, high degree of swelling as well as simple fabrication process.[7,8] So they are promising vehicles in drug delivery systems especially in the intranasal drug delivery system.[9]

Starch microspheres have been synthesized through several approaches,[10-13] among which water-in-oil (W/O) emulsion-cross-linking technique is widely used. However, cross-linked starch microspheres prepared by traditional W/O emulsion-cross-linking technique show relatively large size and broad size distribution,[14, 15] which limit the application in drug delivery systems. Therefore, a new method is desperately expected to develop for the synthesis of starch nanoparticles.

Due to the specific chemical and physical properties, such as low melting point, negligible vapor pressure and non-flammability and recyclability, room-temperature ionic liquids (ILs) have been widely used.[16,17] Studies related with ionic liquid microemulsions in which ILs substitute polar phase, nonpolar phase or surfactant have

been reported, and some inorganic nanomaterials can be prepared in this kind of system.[18-21] Additional, some ILs containing Cl^-, Ac^-, NO_3^- anions have been reported to be capable of dissolving starch.[22-24] For example, it has been reported 1-octyl-3-methylimidazolium acetate ([C_8mim]Ac) can dissolve starch, and also substitute polar phase of microemulsions, So [C_8mim]Ac containing starch may substitute polar phase to form ionic liquid microemulsions. As an important series of ionic liquids 1-alkyl-3-methylimidazolium salts, [$C_n$mim]X have amphiphilicity like traditional cationic surfactant because of their hydrophobic chains and polar imidazolium groups, and have been called "surfactant-like" ionic liquids.[25] In microemulsion systems, Long-chained [$C_n$mim]X can be used as substitute for surfactants to stabilize microemulsions.

In this research, 1-hexadecyl-3-methylimidazolium bromide ([C_{16}mim]Br) and [C_8mim]Ac were simultaneously used as substitutes for surfactants and polar phase to prepare [C_{16}mim]Br/butan-1-ol/cyclohexane/[C_8mim]Ac ionic liquid microemulsions. Then, the structure of microemulsions was studied by pseudo-ternary phase diagram, dynamic light scanning (DLS) and conductivity measurement. To decrease the aggregation of nanoparticles, Octenyl Succinic Anhydride (OSA) starch was used as raw material because of it's hydrophobicity. Starch nanoparticles were prepared with IL/O microemulsion system and characterized by scanning electron microscopy (SEM), dynamic light scattering (DLS), Fourier transform infrared spectroscopy (FTIR). Moreover, the drug loading and releasing properties of starch nanoparticles were studied with mitoxantrone hydrochloride as drug model. There is no report about

the preparation of starch nanoparticles in two ionic liquids based microemulsion system, so this work may provide an efficient and environment method to synthesis starch nanoparticles and broaden the application of starch nanoparticles in medical filed.

2. Material and methods

2.1 Materials

1-hexadecyl-3-methylimidazolium bromide ([C_{16}mimBr], >99%) and 1-octyl-3-methylimidazolium acetate ([C_8mim]Ac, >99%) were purchased from Lanzhou Institute of Chemical Physics (Lanzhou, China). Native corn starch was obtained from ChangChun DaCheng Corn Products Co. (Changchun, China). All other chemicals were of analytical grade.

2.2 Preparation of ionic liquid microemulsion

The preparation of [C_{16}mim]Br/butan-1-ol/cyclohexane/[C_8mim]Ac microemulsion system was conducted by direct visual observation. An appropriate amount of surfactant (0.1937g), [C_8mim]Ac (0.1800g, the mass ratio of [C_8mim]Ac to surfactant ω=0.93), and cyclohexane (1mL) was taken into test tubes, and their masses were determined by an FA1104N analytical balance (Shanghai Balance Instrument Co., Shanghai, China) with a resolution of 0.0001g. Then, the tubes were placed in the thermostatic water bath. The cosurfactant butan-1-ol was slowly added in small intervals to the mixture with constant stirring until the hierarchical and hazy solution

98 became clear, which was indicative of the formation of the single phase.

99

100 **2.3 Pseudo-ternary phase diagram**

101 Fixed amounts of [C_{16}mim]Br, [C_8mim]Ac/water and different amounts of oil were
102 taken into test tubes and kept in a thermostatic water bath at 40℃. The cosurfactant
103 butan-1-ol was slowly added to the mixture until the solution became just clear. The
104 clear point indicated the formation of single-phase system. The same procedure was
105 repeated for 3 times for each mixture, and an average of these results was taken for
106 the pseudo-ternary phase diagram.

107

108 **2.4 Dynamic light scanning**

109 Dynamic light scanning was used to determine the size distribution of
110 [C_{16}mim]Br/butan-1-ol/cyclohexane/[C_8mim]Ac microemulsions and further
111 demonstrate the formation of microemulsions. Measurements were conducted using
112 the Malvern Nano-Zetasizer particle size analyzer (Malvern Instrument Ltd.,
113 Worcestershire, UK) at a wavelength of 633 nm. The scattering angle was set at 90°.

114

115 **2.5 Conductivity measurements**

116 [C_{16}mim]Br and butan-1-ol were mixed as surfactant by the mass ratio of 3:1.
117 [C_8mim]Ac (0.5 g) was added to the mixture of surfactant and cyclohexane each time,
118 and then conductivity values were measured until the solution became turbid. The
119 conductivity of microemulsion was measured using a model DDSJ-308A

conductometer (Shanghai Precision Scientific Instrument Co., Shanghai, China) at 1 kHz using a dip-type cell of cell constant 0.971 cm^{-1}. Conductometer had been corrected by distilled water, and the errors in the conductance measurements were ±0.5%.

2.6 Preparation of OSA modified native corn starch

Native corn starch (10 g, dry weight) was suspended in distilled water (35%, w/w) with agitation, and then placed in a water bath at 35 °C. The pH of the slurry was adjusted to 8.5 with 3% (w/w) NaOH solution. 3% (based on starch dry weight) OSA was added slowly over 2h, and pH was controlled at 8.5 by a pH controller (Model 501-3400, Barnant Co.). The reaction was allowed to continue for a further 1 h, and then pH was adjusted to 6.5 with 3% HCl solution. The mixture was centrifuged, washed two times with distilled water and two times with 70% aqueous alcohol. The sample was oven-dried at 40 °C for 24 h, and passed through a 180 mesh nylon sieve (90 μm opening).

2.7 Determination of degree of substitution (DS)

The degree of substitution (DS) is the average number of hydroxyl groups substituted per glucose unit. The DS of OSA starch was determined by titration. Briefly, 1.5 g of OSA starch was accurately weighed and dispersed in 50 mL of 95% ethanol by stirring for 10 min. Then 15 mL of 2 mol/L HCl alcohol solution was added and the slurry was stirred for a further 30 min. The suspension was filtered

through a glass filter and the residue was washed with 90% alcohol solution until no Cl^- could be detected (using 0.1 mol/L $AgNO_3$ solution). The starch was redispersed in 100 mL of distilled water and cooked in a boiling water bath for 20 min, then titrated with 0.1 mol/L standard NaOH solution using phenolphthalein as an indicator. A blank was simultaneously titrated with native corn starch as a sample.

The DS was calculated as follow:

$$DS = 0.1624A/(1-0.21A) \quad (1)$$

Where A (mmol) is the amount of standard sodium hydroxide solution (0.1 mol/L) consumed by each gram OSA starch.

According to the calculation, the DS of the modified starch was 0.0172.

2.8 Preparation and Characterization of starch nanoparticles

2.8.1 Preparation of starch nanoparticles

Starch nanoparticles were prepared according to IL/O microemulsion-cross-linking method with OSA starch as raw material, epichlorohydrin as cross-linker. This method combined the ionic liquid microemulsion with cross-linking reaction of starch nanoparticles. First, the water phase was prepared by dissolving OSA starch (0.5 g) into $[C_8mim]Ac$ (9.5g), stirred for homogeneous mixing and heated in an oil bath at 135 ℃ for 2.5 h. Then $[C_8mim]Ac$-starch solution and cyclohexane (40g) were added into the small beaker to form IL/O microemulsion with the aid of 20g of the mixture of surfactant $[C_{16}mim]Br$ and cosurfactant butan-1-ol ($[C_{16}mim]Br$/butan-1-ol=3:1, w/w). After the ionic liquid microemulsions containing

OSA starch were formed, epichlorohydrin (1.4 g) was added to the above microemulsion as cross-linker. Then, the mixture was stirred at 50 ℃ for 3 h. The reaction solution was cooled to room temperature and starch nanoparticles were subsequently precipitated with anhydrous ethanol under vigorous stirring followed by centrifugation. The precipitate was washed thoroughly with sufficient anhydrous ethanol to eliminate [C_{16}mim]Br, unreacted epichlorohydrin, butan-1-ol and cyclohexane. Finally, the solid was centrifuged and dried in vacuum at 40 ℃ for 24 h.

2.8.2 Characterization of starch nanoparticles

SEM images of samples were examined by scanning electron microscope (Quanta 200, FEI, Oregon, USA). The accelerating voltage was 20 kV. The samples were mounted on an aluminum stub with double sticky tape, followed coating with the gold in a vacuum before examination.

The particle size and distribution of starch nanoparticles were determined by DLS (Nano ZS, Malvern Instrument Ltd., Worcestershire, UK). Before measuring, 0.01 g of starch nanoparticles were added to 100 mL distilled water and treated by ultrasound for 1h to disperse sufficiently.

The FTIR spectra of samples were recorded on a Nicolet 510 spectrophotometer (Thermo Electron, Waltham, USA) using KBr disk technique. For FTIR measurement, the samples were mixed with anhydrous KBr and then compressed into thin disk-shaped pellets. The spectra were obtained with a resolution of 2 cm^{-1} between a

wave number range of 400–4000 cm^{-1}.

2.9 Drug loading and release properties of starch nanoparticles

2.9.1 Standard curves of mitoxantrone hydrochloride

Standard curves of mitoxantrone hydrochloride in phosphate-buffered saline (PBS, 0.2 mol/L, pH 7.4) were obtained as follow: 0.01 mg/mL of mitoxantrone hydrochloride in PBS solution was scanned at the wavelength between 400~800nm with ultraviolet–visible spectrophotometer (TU-1901, Beijing Puxi General Apparatus, Ltd., China). The wavelength at which mitoxantrone hydrochloride absorbed the most was selected as the testing wavelength for later experiments. Then, 0.01, 0.02, 0.04, 0.08, 0.10 and 0.12mg/mL of mitoxantrone hydrochloride in PBS solution were measured at their corresponding testing wavelengths to obtain standard curves of mitoxantrone hydrochloride absorbance to concentration for each solution.

2.9.2 Drug loading analysis

About 0.1 g of starch nanoparticles were weighed and suspended in 20 mL of PBS solution with 0.02 0.04, 0.08, and 0.12 mg/mL of mitoxantrone hydrochloride each. The resulting suspensions were gently stirred at the desired temperature of 17, 27, 37, and 47 °C for 0.5, 1, 1.5, 2 and 2.5 h, respectively. Then, the solutions were centrifuged, and 1 mL of each supernatant was extracted and diluted to certain volume to determine the drug loading amount and encapsulation efficiency according to the standard curve of mitoxantrone hydrochloride absorbance. The drug loading amount

(A) and encapsulation efficiency (B) were calculated with the following equations, respectively.

$$A = (C_0 - C_1V_1)V_0 / W \quad (2)$$

$$B = (C_0 - C_1V_1) / C_0 \quad (3)$$

Where C_0 means initial concentration of mitoxantrone hydrochloride in PBS solution, C_1 means diluted concentration of mitoxantrone hydrochloride in PBS solution, V_1 means dilution volume of extracted supernatant, V_0 means initial volume of PBS solution, and W means the weight of starch nanoparticles dissolved in PBS solution.

2.9.3 Drug release analysis

About 0.1 g of drug-loaded starch nanoparticles that possessed the most drug loading (4.97 mg/g) under the experimental conditions above were weighed and added to the dialysis tube. Then, 10 mL of phosphate buffer solution (PBS, pH=7.4) was added to the dialysis tube. Subsequently, the drug-loaded starch nanoparticles and dialysis tube were placed in a beaker containing 90 mL of PBS and slowly stirred in magnetic stirring apparatus at 37 °C. 5 mL of PBS solution with starch nanoparticles was taken out and the sample drawn was replaced by fresh PBS to maintain a constant volume. The cumulative release rate was determined according to the standard curve of mitoxantrone hydrochloride absorbance to concentration and Eq (4).

$$R = M_1 / M_0 \quad (4)$$

Where M_1 is the cumulative mass of mitoxantrone hydrochloride released from

drug-loaded starch nanoparticles at a given time, and M_0 is the total drug loading amount in starch nanoparticles.

2.9.4 Statistical analysis

All of the sample analyses were conducted in triplicate and the values were expressed as means ± standard error of the mean, Statistical analysis were done using SPSS 18.0. Duncan's multiple range tests were used to estimate significant differences among means at a probability level of 0.05.

3 Results and discussion

3.1 Pseudo-ternary phase diagram

The pseudo-ternary phase diagram of the [C_{16}mim]Br/butan-1-ol /cyclohexane/[C_8mim]Ac (water) microemulsion system with fixed ω value (ω=0.93) at 40℃ is shown in **Fig. 1**. Apparently, two different regions, a single-phase region (1Φ) and a two-phase region (2Φ), could be observed. The single phase region contained IL/O (W/O) microemlusion. In addition, when [C_8mim]Ac replaced water phase to form microemulsion, the single phase region grew, which indicated that [C_8mim]Ac as water phase was more beneficial to the formation of the single phase microemulsion compared with water.

3.2 Dynamic light scanning

The size distribution of the droplets in the IL/O microemulsion was characterized

by DLS. A series of [C_{16}mim]Br/butan-1-ol/cyclohexane/[C_8mim]Ac microemulsions with different R values (the mass ratio of [C_8mim]Ac to cyclohexane) were chosen for DLS analysis. As shown in **Fig. 2**, the sizes of microemulsions increased from about 3.1 to 13.4 nm with increasing R values from 1:9 to 4:6. The microemulsions showed regular swelling behavior with the increase of [C_8mim]Ac, which indicated the formation of IL/O microemulsion according to the studies by Pramanik *et al*. and Gao *et al*..[26, 27]

3.3 Conductivity measurements

In this work, IL/O microemulsions system was chosen as the cross-linking reaction system for the preparation of starch nanoparticles. The conductivity measurements were widely used to determine the structure of microemulsions. According to the percolation conductance model, with the increase of [C_8mim]Ac, conductivity curve can be divided into three segments: the sharp rise, flat and the drop of last, corresponding to three ultrastructural structures of microemulsions droplets IL/O, BC (Bicontinuous Cubic) and O/IL, respectively.[28] As shown in **Fig. 3**, for the mass ratio of surfactant to cyclohexane 2:8, 3:7 and 4:6, the conductivities of microemulsions all rose sharply with the increase of [C_8mim]Ac. Therefore, only IL/O microemulsions formed when the mass ratio of surfactant to cyclohexane was between 2:8 and 4:6.

3.4 SEM analysis

The morphologies of OSA starch and starch nanoparticles were observed by SEM. As shown in **Fig. 4**, OSA starch granules were polygonal or irregular shapes and the surface was rough. Compared with OSA starch, starch nanoparticles were spherical granules and much smaller than OSA starch. In addition, compared with starch nanoparticles prepared by Liu *et al.* and Zhou *et al.*,[29, 30] the particles presented more homogeneous distribution and no aggregation phenomenon appeared.

3.5 Particle size and distribution of starch nanoparticles

DLS was used to measure the particle size and distribution of starch nanoparticles. As we can see from **Fig. 5**, starch nanoparticles had a relatively concentrated size distribution and the mean diameter was 80.5 nm, which was much smaller than that of starch microspheres prepared by the traditional W/O emulsion cross-linking method.[31] The result of DLS was also consistent with the data in **Fig. 4**. So IL/O microemulsion-cross-linking method is an ideal way to produce starch nanoparticles with a relatively concentrated distribution and smaller size.

3.6 FTIR analysis

The FTIR spectra of OSA starch and starch nanoparticles are shown in **Fig. 6**. For the FTIR spectrum of OSA starch, the extremely broad band at 3400 cm^{-1} and the peak at 2926 cm^{-1} corresponded to O-H and C-H stretching, respectively. Two characteristic peaks at 1727, and 1570 cm^{-1} were attributed to C=O and C=C stretching vibrations of OSA starch, respectively. Meanwhile, the band at 1645 cm^{-1}

was assigned to O–H bending vibration. Besides, other bonds at 1156, 1081, and 1018 cm^{-1} were attributed to the C–O bond stretching vibrations of anhydroglucose units. Compared with OSA starch, the spectra of starch nanoparticles exhibited some difference. The absorption peak at 3456 cm^{-1} became lankier and shifted slightly to high frequency regions,[32] which was due to the weakening of the hydrogen band connection in cross-linking reaction. In addition, the peak at 1727 cm^{-1} disappeared, the peaks at 1654 and 1581cm^{-1} became much weaker, and the peaks at 1174, 1094 and 1032cm^{-1} changed and band intensity got stronger. All these results suggested that cross-linking bonds were formed between starch molecules. Similar result was also reported by Mundargi when they studied the FTIR of starch microspheres[8].

3.7 Drug loading analysis

According to the scanning results, the testing wavelengths of mitoxantrone hydrochloride were 610 nm. Moreover, standard curve of mitoxantrone hydrochloride absorbance to concentration (from 0.01 to 0.12 mg/mL) in PBS solution was $A=25.43C+0.013$，$R^2=0.999$.

The effect of loading time on drug loading amount and encapsulation efficiency is shown in **Table 1**. As shown in **Table 1**, with the lengthening of loading time, the drug loading amount and enhanced encapsulation efficiency of mitoxantrone hydrochloride increased first and then decreased between 0.5 and 2.5 h ($P<0.05$). To be more exact, the drug loading amount increased from 0.52 to 0.98 mg/g and encapsulation efficiency rose from 6.52 to 12.43% when the loading time extended

from 0.5 to 1.5 h. However, with the time extending from 2.0 to 2.5 h, the drug loading amount and encapsulation efficiency decreased to 0.46 mg/g and 5.75%, respectively. Therefore, it can be concluded that the optimal loading time was 1.5 h.

As shown in **Table 2**, loading temperature affected drug loading amount and encapsulation efficiency of mitoxantrone hydrochloride to some extent (P<0.05). The drug loading amount encapsulation efficiency ascended with the rise of loading temperature from 17 to 27°C and reached the maximum at 27°C. The reason was that the sorption of mitoxantrone hydrochloride was mainly attributed to the existence of opposite charges and high affinity,[30] which would be blocked by high temperature. So with the loading temperature reaching 47 °C, the drug loading amount and encapsulation efficiency reduced to only 2.73 mg/g and 16.84%, respectively.

The effect of mitoxantrone hydrochloride concentration on the drug loading amount and encapsulation efficiency is depicted in **Table 3**, which revealed that the rise in mitoxantrone hydrochloride concentration facilitated drug loading amount significantly (P<0.05). However, encapsulation efficiency increased first and then decreased with the concentration of mitoxantrone hydrochloride rising from 0.02 to 0.12 mg/mL and the maximum encapsulation efficiency attained 21.22% when the concentration of mitoxantrone hydrochloride reached 0.08 mg/mL. Therefore, higher mitoxantrone hydrochloride concentration did not facilitate drug loading property.

3.8 Drug release analysis

The mitoxantrone hydrochloride release property of starch nanoparticles is

presented in **Fig. 7**. Initially, a significant release could be clearly observed after the drug-loaded starch nanoparticles were immersed into PBS solution. High release rate of 54.36% in the first 1 h was assigned to the immediate dispersing of mitoxantrone hydrochloride close to the starch microspheres surfaces. In the next 9 h, the drug-loaded starch nanoparticles formed a swelling-controlled and sustained release system, in which the release rate showed a slight but slow rise. 91.47% of MB contained in the starch nanoparticles was released in the 10th hour, and the release of mitoxantrone hydrochloride reached a balance between starch microspheres and PBS solution, only tiny amount of mitoxantrone hydrochloride was released due to the sluggish degradation of starch particles. These observed results were consistent with that of Fang et al.[15] when they studied the release property of starch microsphere.

4 Conclusions

This work described an exploratory research on the preparation of starch nanoparticles based on a novel ionic liquid microemulsion system and the drug loading and releasing properties of starch nanoparticles. $[C_{16}mim]Br$/butan-1-ol/cyclohexane/$[C_8mim]Ac$ ionic liquid microemulsions was prepared. Then, the structure of microemulsions was identified by pseudo-ternary phase diagram, DLS and conductivity measurement. Starch nanoparticles were prepared with IL/O microemulsion system as reaction system and OSA starch as raw material. SEM results revealed that starch nanoparticles were spherical granules with small size, in addition, the particles presented more homogeneous distribution and no

aggregation phenomenon appeared. DLS date showed the mean diameter of starch nanoparticles was 80.5 nm. The formation of cross-linking bonds between starch molecules was identified by FTIR. In terms of drug loading property of starch nanoparticles, it was found that the drug loading and encapsulation efficiency were influenced by loading time, loading temperature, and drug concentration to some extent (P<0.05). The release curve of drug-loaded starch nanoparticles contained two phases: an initial burst release phase and a sustained release phase.

Acknowledgements

This research was supported by the National Natural Science Foundation of China (21376097, 21576098, 21004023), the program for New Century Excellent Talents in University (NCET-13-0212), the Guangdong Natural Science Foundation (S2013010012318), the Key Project of Science and Technology of Guangdong Province (2015A020209015, 2014A020208016, 2013B090500013), the Key Project of Science and Technology of Guangzhou City (201508020082,2014J4500012), the National Natural Science Fund of China (Foundation of Guangdong Province of China; U1401235), the Fundamental Research Funds for the Central Universities, SCUT (2015ZZ0070, 2014ZZ0052).

References

1 L.M. Che, D. Li, L.J. Wang, N. Özkan, X.D. Chen and Z.H. Mao, *Int. J. Food Prop.*, 2007, **10**, 911-922.

2 R.F. Tester, J. Karkalas and X. Qi, *J. Cereal Sci.*, 2004, **39**, 151–165.

3 Z.G. Luo and Z.Y. Xu, *LWT-Food Sci. Technol.*, 2011, **44**, 1993–1998.

4 S. Jobling, *Current Opin Plant Biol.*, 2004, **7**, 210−218.

5 C.S. Raina, S. Singh, A.S. Bawa and D.C.A. Saxena, *Food Sci. Technol.*, 2007, **40**, 885−892.

6 X.X. Lu, Z.G. Luo, S.J. Yu and X. Fu, *J. Agric. Food Chem.*, 2012, **60**, 9273-9279.

7 M. Kim and S.J. Lee, *Carbohydr. Polym.*, 2002, **50**, 331–337.

8 R.C. Mundargi, N.B. Shelke, A.P. Rokhade, S.A. Patil and T.M. Aminabhavi, *Carbohydr. Polym.*, 2008, **71**, 42–53.

9 S.R. Mao, Z.M. Chen, Z.P. Wei, H. Liu and D.Z. Bi, *Int. J. Pharm.*, 2004, **272**, 37–43.

10 J.M. Bezemer, R. Radersma, D.W. Grijpma, P.J. Dijkstra, C.A. Van Blitterswijk and J. Feijen, *J. Contro. Release.*, 2000, **67**, 233–248.

11 M. Kawashitaa, M. Tanakab, T. Kokuboc, Y. Inoued, T. Yaoe and S. Hamadaf, *Biomaterials*, 2005, **26**, 2231–2238.

12 M. Luck, K.F. Pistel, Y.X. Li, T. Blunk, R.H. Muller and T. Kissel, *J. Contro. Release.*, 1998, **55**, 107–120.

13 C. Sturesson and J. Carlfors, *J. Contro. Release.*, 2000, **67**, 171–178.

14 O. Franssen and W.E. Hennink, *Int. J. Pharm.*, 1998, **168**, 1−7.

15 Y.Y. Fang, L.J. Wang, D. Li, B.Z. Li, B. Bhandari, X.D. Chen and Z.H. Mao, *Carbohydr. Polym.*, 2008, **74**, 379−384.

16 R. Sheldon, *Chem. Rev.*, 2001, **23**, 2399–2407.

406 17 T. Welton, *Chem. Rev.*, 1999, **99**, 2071–2083.

407 18 S.Q. Cheng, X.G. Fu, J.H. Liu, J.L. Zhang, Z.F. Zhang and Y.L. Wei, *Colloids Surf.*

408 *A*, 2007, **302**, 211−215.

409 19 S.Q. Cheng, F. Han, Y.R. Wang and J.F. Yan, *Colloids Surf. A*, 2008, **317**, 457−461.

410 20 H.X. Gao, J.C. Li, B.X. Han, W.N. Chen, J.L. Zhang, R. Zhang and Y.D. Yan, *Phys.*

411 *Chem. Chem. Phys.*, 2004, **6**, 2914−2916.

412 21 F. Yan and J. Texter, *Chem. Commun.*, 2006, **25**, 2696−2698.

413 22 Q. Liu, M.H.A. Janssen, F. Van Rantwijk and R. Sheldon, *Green Chem.*, 2005, **7**,

414 39–42.

415 23 A.A. Rosatella, L.C. Branco and C.A.M. Afonso, *Green Chem.*, 2009, **11**,

416 1406–1413.

417 24 R.L. Shogren and A. Biswas, *Carbohydr. Polym.*, 2010, **81**, 149–151.

418 25 S. Thomaier and W. Kunz, *J. Mol. Liq.*, 2007, **130**, 104-107.

419 26 R. Pramanik, C. Ghatak, V.G. Rao, S. Sarkar and N.J. Sarkar, *J. Phys. Chem. B*,

420 2011, **115**, 5971−5979.

421 27 Y. Gao, S. Han, B. Han, G. Li, D. Shen, Z. Li, J. Du, W. Hou and G. Zhang,

422 *Langmuir*, 2005, **21**, 5681–5684.

423 28 M. Lagues, M. Dvolaitzky, J.P. Le Pesant and R. Ober, *J. Phys. Chem.*, 1980, **84**,

424 1532-1535.

425 29 J. Liu, F.H. Wang, L.L. Wang, S.Y. Xiao, C.Y. Tong, D.Y. Tang and X.M. Liu, *J.*

426 *Cent. South Univ. Technol.*, 2008, **15**, 768-773.

427 30 G. Zhou, Z.G. Luo, X. Fu, *J. Agric. Food Chem.*, 2014, **62**, 8214-8220.

31 X.F. Zhao, Z.J. Li, L. Wang and X.J. Lai, *J. Appl. Polym. Sci.*, 2008, **109**, 2571−2575.

32 Y.T. Yang, X.Z. Wei, P. Sun and J.M. Wan, *Molecules*, 2010, **15**, 2872-2875.

Table 1 Effect of loading time on mitoxantrone hydrochloride loading.

Loading time (h)	Drug loading amount (mg/g)	Encapsulation efficiency (%)
0.5	$0.52\pm0.025^{C,D}$	6.52 ± 0.055^{D}
1	0.70 ± 0.040^{B}	8.75 ± 0.060^{B}
1.5	0.98 ± 0.045^{A}	12.43 ± 0.075^{A}
2	0.58 ± 0.045^{C}	7.45 ± 0.055^{C}
2.5	0.46 ± 0.030^{D}	5.75 ± 0.040^{E}

Values represent the means ± SD; n = 3. Values in a column followed by different capital letters as superscripts were significantly different from each other according to Duncan's multiple range tests ($p < 0.05$).

435 **Table 2** Effect of loading temperature on mitoxantrone hydrochloride loading.

Loading temperature (°C)	Drug loading amount (mg/g)	Encapsulation efficiency (%)
17	3.44 ± 0.045^{B}	21.32 ± 0.345^{B}
27	3.75 ± 0.055^{A}	23.17 ± 0.281^{A}
37	3.26 ± 0.065^{C}	20.15 ± 0.400^{C}
47	2.73 ± 0.035^{D}	16.84 ± 0.211^{D}

436 Values represent the means ± SD; n = 3. Values in a column followed by different
437 capital letters as superscripts were significantly different from each other according to
438 Duncan's multiple range tests ($p < 0.05$).

439 **Table 3** Effect of mitoxantrone hydrochloride concentration on drug loading.

Drug concentration (mg/mL)	Drug loading amount (mg/g)	Encapsulation efficiency (%)
0.02	0.46 ± 0.050^{D}	11.53 ± 0.242^{C}
0.04	0.92 ± 0.041^{C}	12.59 ± 0.285^{B}
0.08	3.36 ± 0.074^{B}	21.22 ± 0.215^{A}
0.12	4.97 ± 0.045^{A}	20.96 ± 0.180^{A}

440 Values represent the means ± SD; n = 3. Values in a column followed by different
441 capital letters as superscripts were significantly different from each other according to
442 Duncan's multiple range tests ($p < 0.05$).

443 **Figure captions**

444 **Fig.1** Pseudo-ternary phase diagrams of [C_{16}mim]Br/butan-1-ol/cyclohexane/water (A)
445 and [C_{16}mim]Br/butan-1-ol/cyclohexane/[C_8mim]Ac (B) microemulsion systems.

446

447 **Fig.2** Size distribution of [C_{16}mim]Br/butan-1-ol/cyclohexane/[C_8mim]Ac
448 microemulsions. ω represents the mass ratio of [C_8mim]Ac to cyclohexane.

449

450 **Fig.3** The conductivity of microemulsion system with the different mass ratio of
451 surfactant and cyclohexane.

452

453 **Fig.4** SEM of OSA starch×1000 (A) and starch particles×40000 (B).

454

455 **Fig.5** The particle size and distribution of starch nanoparticles.

456

457 **Fig.6** FTIR of OSA starch (a) and starch nanoparticles (b).

458

459 **Fig.7** Mitoxantrone hydrochloride release of starch nanoparticles in PBS solution

460

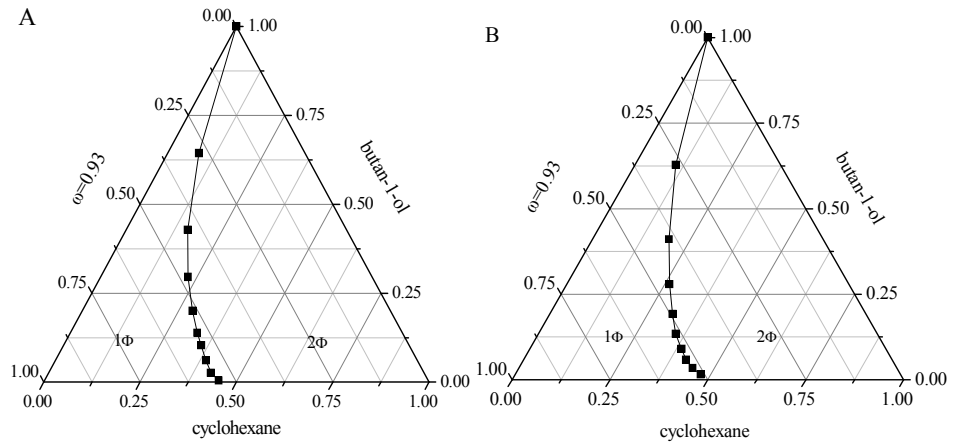

Fig. 1 Pseudo-ternary phase diagrams of [C_{16}mim]Br/butan-1-ol/cyclohexane/water (A) and [C_{16}mim]Br/butan-1-ol/cyclohexane/[C_8mim]Ac (B) microemulsion systems.

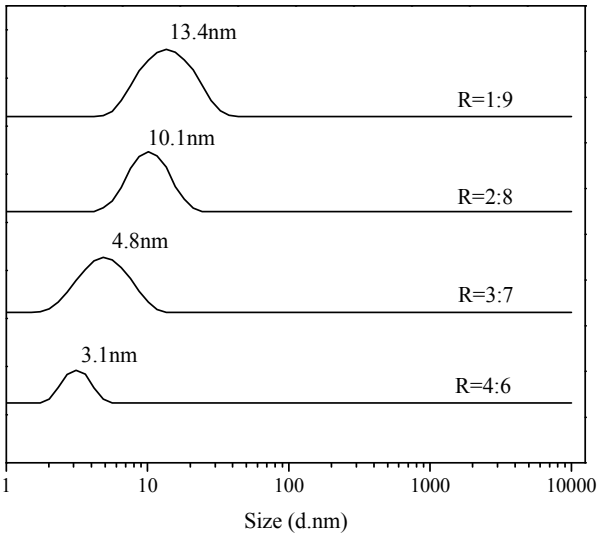

464

465 **Fig. 2** Size distribution of [C_{16}mim]Br/butan-1-ol/cyclohexane/[C_8mim]Ac

466 microemulsions. R represents the mass ratio of [C_8mim]Ac to cyclohexane.

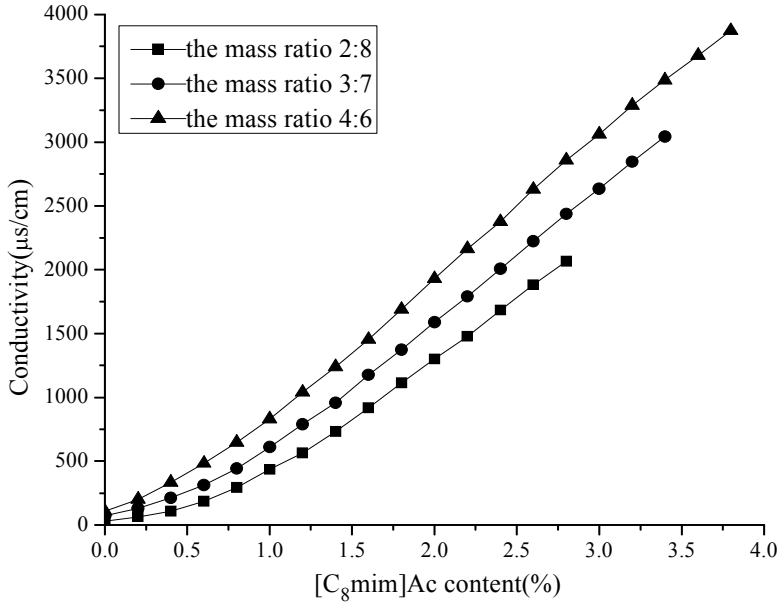

Fig. 3 The conductivity of microemulsion system with the different mass ratio of surfactant to cyclohexane.

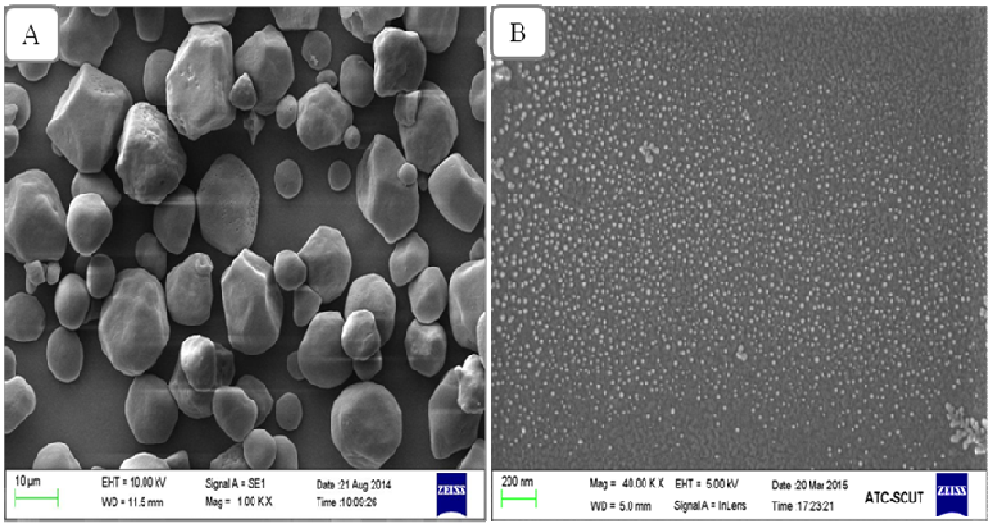

Fig. 4 SEM of OSA starch×1000 (A) and starch nanoparticles×40000 (B).

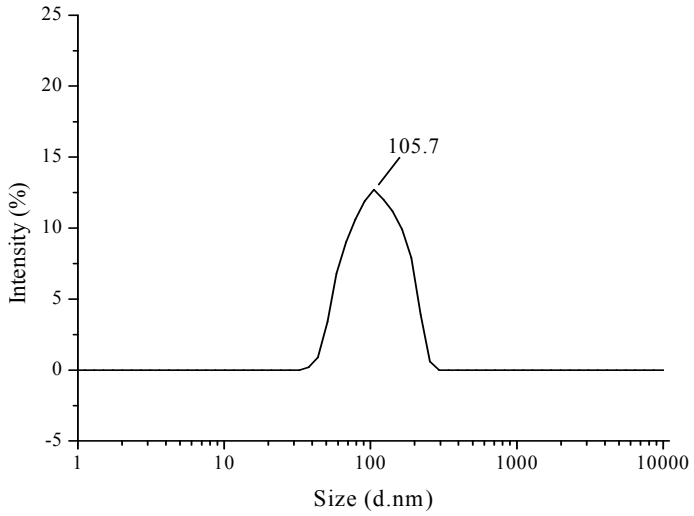

Fig. 5 The particle size and distribution of starch nanoparticles.

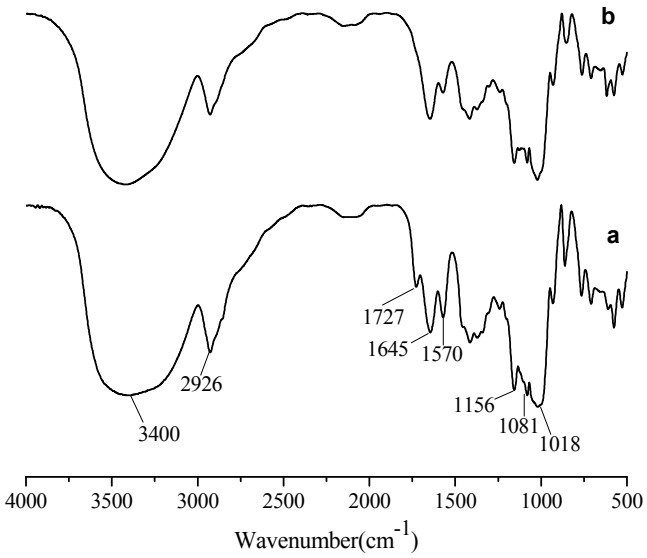

474

475 **Fig. 6** FTIR of OSA starch (a) and starch nanoparticles (b).

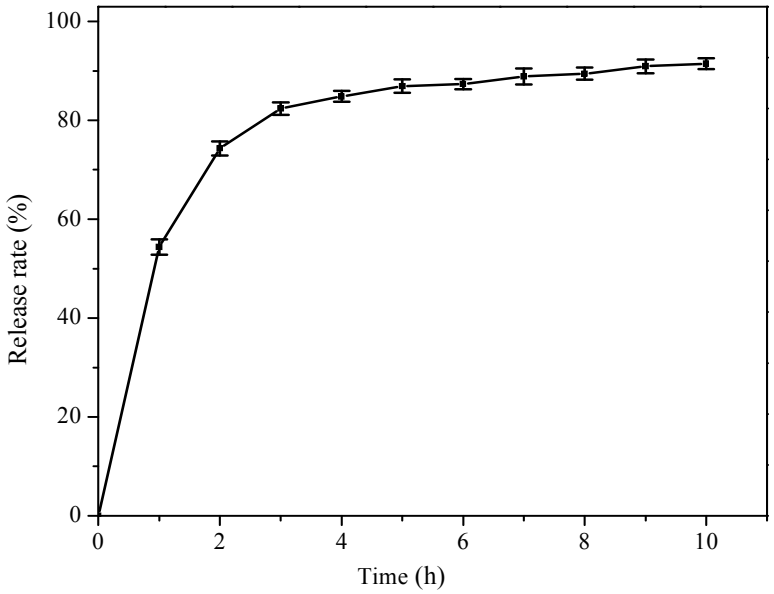

476

477 **Fig. 7** Mitoxantrone hydrochloride release of starch nanoparticles in PBS solution.

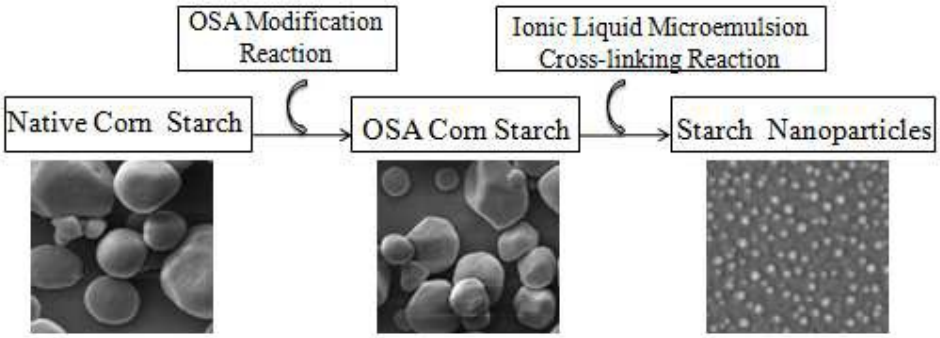

Graphical abstract